PAPER

Check for updates

Nanoarchitectonics of carbon molecular sieve membranes with graphene oxide and polyimide for hydrogen purification

Wen He, Jingcheng Du, Linghao Liu, Qian Sun, Ziye Song, Ji Ma, Dong Cao, Weiwang Lim, Shabi Ul Hassan and Jiangtao Liu [ID] *

Hydrogen is an important energy carrier for the transition to a carbon-neutral society, the efficient separation and purification of hydrogen from gaseous mixtures is a critical step for the implementation of a hydrogen economy. In this work, graphene oxide (GO) tuned polyimide carbon molecular sieve (CMS) membranes were prepared by carbonization, which show an attractive combination of high permeability, selectivity and stability. The gas sorption isotherms indicate that the gas sorption capability increases with the carbonization temperature and follows the order of PI–GO-1.0%-600 °C > PI–GO-1.0%-550 °C > PI–GO-1.0%-500 °C, more micropores would be created under higher temperatures under GO guidance. The synergistic GO guidance and subsequent carbonization of PI–GO-1.0% at 550 °C increased H_2 permeability from 958 to 7462 Barrer and H_2/N_2 selectivity from 14 to 117, superior to state-of-the-art polymeric materials and surpassing Robeson's upper bound line. As the carbonization temperature increased, the CMS membranes gradually changed from the turbostratic polymeric structure to a denser and more ordered graphite structure. Therefore, ultrahigh selectivities for H_2/CO_2 (17), H_2/N_2 (157), and H_2/CH_4 (243) gas pairs were achieved while maintaining moderate H_2 gas permeabilities. This research opens up new avenues for GO tuned CMS membranes with desirable molecular sieving ability for hydrogen purification.

1. Introduction

Global warming is one of the most important challenges today that all mankind is facing and needs to be solved urgently. The key to meeting this challenge is to consistently expand the renewable energy sources. With the growing demand of global energy and environmental protection, hydrogen energy has been considered as one of the most promising alternatives to traditional fossil fuels and offers the potential to effectively alleviate the serious energy crisis and green-house effect owing to its distinct advantages such as abundant sources, high energy density and clean combustion without carbon emission.[1,2] However, the produced H_2 stream usually contains a significant amount of N_2, CH_4, and CO_2 that should be removed to produce high purity hydrogen. Purification of hydrogen from this gas stream requires novel separation technologies to improve energy efficiency as it consumes 60% of the total energy requirement in the whole hydrogen production process. The state-of-the-art hydrogen purification technologies of pressure swing adsorption (PSA) and cryogenic distillation, are energy-intensive, while membrane gas separation technology shows its potential in this application because of its low energy

consumption, easy operation and maintenance, small footprint, and environmental friendliness.[3–6] Various materials such as polymeric membranes,[7,8] inorganic membranes such as graphene oxide (GO),[9] MoS_2,[10] metal–organic frameworks (MOFs),[11,12] zeolite imidazolate framework (ZIF),[13,14] 2D covalent organic frameworks,[15] and carbon membranes[16] have been explored for H_2 separation. However, the main disadvantages of the above membranes are low gas permeability as well as poor selectivity, since they usually exhibit a trade-off constraint.[17,18] In addition, the physical aging problem and CO_2 plasticization must also be solved during the long-term service under adverse conditions (*e.g.*, high temperature and pressure in the steam methane reforming process).[19,20]

Carbon molecular sieve (CMS) membranes have gained much attention due to their high separation performance, excellent thermal stability, and chemical resistance.[21–27] CMS membranes with strong carbon structures are typically fabricated by controlled carbonization of polymeric precursors at high temperature. During the thermal treatment process, the disordered polymeric structures tend to form ordered slit-like carbon structures as the pathway for H_2 gas transport.[28,29] Different kinds of polymeric materials, including polyimide and its derivatives,[30–34] cellulose and its derivatives,[35] poly(arylene ether ketone),[36–38] poly(phenylene oxide)[39,40] and poly-benzimidazole,[41] have been employed as the precursors to

Department of Environmental Science and Engineering, University of Science and Technology of China, 230052, China. E-mail: jiangtaoliu@ustc.edu.cn

fabricate CMS membranes for H_2 purification. Compared to pristine polymeric membranes, CMS membranes have excellent gas separation performance for hydrogen purification, which can exceed the Robeson upper bounds of polymeric membranes that plot a trade-off relationship between the gas permeability and selectivity. Furthermore, CMS membranes exhibit higher thermal stability and better plasticization resistance. Previous research has provided guidance for the structural design of polymeric precursors, the polymeric chain properties such as conformation, rigidity and packing efficiency also have a great effect on the gas separation performance of the CMS membrane. Therefore, great efforts have been devoted to exploring novel polymeric precursors to prepare CMS membranes with high gas permeability and good selectivity. High permeability is beneficial to reduce investment costs and good selectivity will meet the demand for high purity. Tseng et al.[42] found that the functional groups of precursors (polyimide versus polyetherimide) and their thermal stability could be optimized to enhance the H_2 separation properties of CMS membranes. Cao et al.[37] reported that the chemical structure (sulfone/ketone unit ratio) of copolymer precursors had a significant influence on the H_2 separation performance. Ma et al.[31] believed that the configuration of monomer prominently affected the polyimide properties, leading to great differences among the CMS membranes. Koros et al.[43] and Lee et al.[44] reported that reducing the chain packing (or enhancing the FFV) of polymeric precursors by introducing monomers with bulky side groups could enhance the gas permeability. Pinnau et al.[45] found that the rigid and contorted aromatic structure was beneficial for reducing the shrinkage of micropores when the membranes were pyrolyzed at high temperatures. These previous works investigated the effect of chemical structure on H_2 permeability and selectivity of CMS membranes.[46]

Until now, the incorporation effect of 2D nanofillers into polymer matrix has not been fully explored. Graphene-based 2D materials, such as graphene and graphene oxide, have been considered promising membrane materials, because they are only one carbon atom thick and, thus, may offer a wide range of opportunities for membrane with minimize transport resistance and maximize flux. Additionally, they have good stability and strong mechanical strength. Therefore, in this work, the CMS membranes were fabricated via the in situ incorporation of GO into the polymeric membranes. The aims of this study were to explore the science and engineering that 2D GO in the polymer matrix can (1) regulate the packing of polymer chains, (2) restructure the architecture, (3) manipulate the free volume with enhanced gas separation performance, and (4) improve the resistance to physical aging and CO_2 plasticization problems.

2. Experimental

2.1. Materials

The monomer 4,4'-(hexafluoroisopropylidene)diphthalic anhydride (6FDA) was obtained from Clariant and 2,3,5,6-tetramethyl-1,4-phenylenediamine (Durene diamine) was purchased from Sigma-Aldrich. The graphene oxide (GO) aqueous solution of 0.5 wt% was purchased from Angstron

Materials Inc. The analytical grade N,N'-dimethylformamide (DMF, >99.5%) and N-methyl-2-pyrrolidone (NMP, >99.5%) were purchased from Sinopharm Chemical Reagent Co., Ltd. The methanol (MeOH, ≥99.9%), ethanol (EtOH, ≥99.9%), and other solvents were ordered from Sinopharm Chemical Reagent Co. Ltd. and used as received. The high purity gases H_2 (>99.999%), CO_2 (>99.999%), N_2 (>99.999%), and CH_4 (>99.999%) were supplied by Nanjing Shangyuan Industrial Gas Factory (Jiangsu, China). Petri dishes and glass sheets were purchased from Shanghai Glass Instrument Factory (Shanghai, China).

2.2. Fabrication of 6FDA–durene membrane

The typical procedure for the fabrication of 6FDA–durene membrane was carried out as follows: a stoichiometric amount of 6FDA was added to NMP solution consisting of durene at an equal molar ratio in a moisture free flask with stirring and nitrogen inlet at room temperature. After reaction for 24 h, a high molecular weight polyamic acid was formed, and then the polyamic acid solution was cast in Petri dishes at ambient temperature in fume hood. The thin layer of the solution was then covered by a tin foil to allow the slow evaporation of NMP. The thermal imidization of polyamic acid was performed in vacuum under the stepwise heating at 100, 200 and 250 °C for 60, 60 and 30 min, respectively. A polyimide film was formed after most of the solvent had evaporated in the vacuum oven. The nascent membrane was then peeled off and the average thickness of the membranes was measured from 10 different points using a Digimatic indicator with an accuracy of 1 μm. The thicknesses of polyimide membranes were approximately 50 ± 5 μm. The synthetic scheme and chemical structure of polyimide are shown in Fig. 1.

2.3. In situ fabrication of 6FDA–durene–GO membranes

To improve the compatibility between GO and the polymer substrate, a stoichiometric amount GO nanosheets was firstly interact with durene in NMP solution for 24 h. After that the 6FDA in NMP solution was added partially 3 times. The mixture consisting of GO, durene, and 6FDA at stoichiometric molar ratio was stirred in a moisture free flask, and the whole system was purged with N_2 at room temperature. After reaction for 24 h, a high molecular weight polyamic acid–GO solution was formed, and then the polyamic acid–GO solution was cast in a Petri dish at ambient temperature in a fume hood. The thin layer of the solution was then covered by a tin foil to allow the slow evaporation of NMP. The thermal imidization process of polyamic acid was performed in a vacuum oven under the stepwise heating at 100, 200 and 250 °C for 60, 60 and 30 min, respectively. A polyimide–GO-1.0% film was formed after most of the NMP solvent evaporated in the vacuum oven. The nascent membrane was then peeled off and the average thickness of the membranes was measured from 10 different points using a Digimatic indicator with an accuracy of 1 μm. The thicknesses of PI–GO-1.0% membranes were around 50 ± 5 μm. The synthetic scheme and chemical structure of PI–GO are shown in Fig. 1.
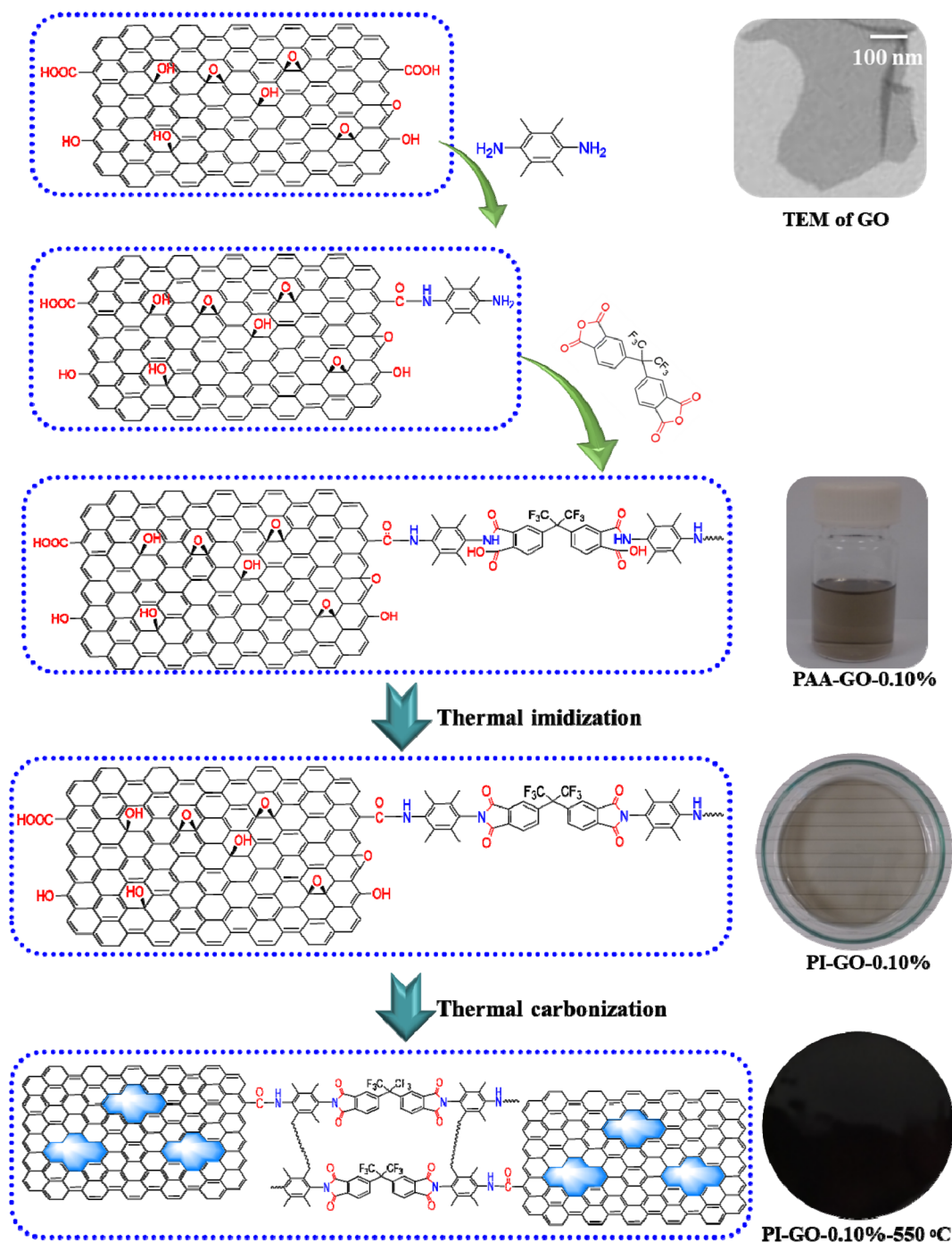
Fig. 1 The structure change and fabrication process from PAA–GO-0.10% to PI–GO-0.10%, and thermal carbonized PI–GO-0.10%-550 °C.

2.4. Characterizations

The chemical structures of 6FDA–durene and 6FDA–durene–GO were analyzed by the attenuated total reflection Fourier transform infrared (ATR-FTIR) spectroscopy 8400 spectrometer in the range of 400–4000 cm^{-1}. The spectra were obtained with an average of 32 scans at a resolution of 4 cm^{-1} and the samples for testing were membranes. The interchain spacings of the polymeric membranes were investigated by a Bruker D8 Advance X-ray diffractometer (XRD), and general area detector diffraction system (GADDS), utilizing Cu K-α as the X-ray radiation source with a wavelength of 1.54 Å. The X-ray diffraction angles between 5 and 30° were studied. The average d-space was evaluated based on the Bragg's law ($n\lambda = 2d\sin\theta$), where n is an integer (1, 2, 3), l represents the X-ray wavelength, d represents the intersegmental spacing between two polymer chains and θ denotes the X-ray diffraction angle. The thermal stability was characterized under a nitrogen atmosphere with a flow rate of 50 mL min^{-1} by thermogravimetric analysis (TGA). A Shimadzu

Thermal Analyzer (DTG-60AH/TA-60WS/FC-60A) was used for these characterizations with a heating rate of 10 °C min⁻¹ from 50 °C to 800 °C. The mechanical properties were tested with at least five film specimens (30 mm long, 5 mm wide, and about 0.05 mm thick) by an Instron model 5542.

2.5. Measurements of gas permeation

Both pure gas and mixed gas permeation of the membranes were conducted on a variable-pressure constant-volume gas permeation cell. The film of dense membrane was mounted onto the permeation cell and vacuumed at 35 °C for 12 h before the gas permeation test was carried out. Pure gas permeability was tested following the order of H_2, O_2, N_2, CH_4, and CO_2. The cell temperature was kept constant at 35 °C. The gas permeability coefficient through the membrane was calculated according to the steady state pressure increment (dp/dt) in the following eqn (4):

$$P = \frac{273 \times 10^{10}}{760} \frac{Vl}{AT\left(p_2 \times \frac{76}{14.7}\right)} \frac{dp}{dt} \tag{1}$$

where P denotes the gas permeability coefficient in Barrer (1 Barrer = 1×10^{-10} cm³ (STP) cm cm⁻² s⁻¹ cmHg⁻¹), V refers to the volume of the downstream reservoir (cm³), A is the effective membrane area (cm²), l represents the membrane thickness (cm), T is the testing temperature (K) and p_2 is defined as the upstream pressure of the system (atm). The permeability tests were repeated at least three times and the average deviation obtained was less than 5%.

The ideal selectivity ($\alpha_{A/B}$, gas A over gas B) between two different gases in a polymeric membrane is the ratio of the permeability of single gas as described in the equation as follows:

$$\alpha_{A/B} = \frac{P_A}{P_B} \tag{2}$$

where p_A and p_B refer to the permeability coefficients of gases A and B, respectively. According to the solution-diffusion model, permeability is the product of diffusivity (D) and solubility (S). Therefore, the ideal permeability selectivity (α_P) can be defined as the product of diffusivity selectivity (α_D) and solubility selectivity (α_S) as follows:

$$P = D \times S \tag{3}$$

$$\alpha_{A/B} = \alpha_P = \alpha_D \times \alpha_S = \frac{D_A}{D_B} \times \frac{S_A}{S_B} \tag{4}$$

where D_A and D_B are the diffusivity coefficients of gases A and B, respectively (cm² s⁻¹); S_A, and S_B are the solubility coefficients of gases A and B, respectively (cm³ (STP) cm⁻³ polymer atm).

The mixed gas permeation properties were evaluated using a binary 50 mol% H_2 and 50 mol% N_2 mixtures. For binary gas separation measurements, the pure gas permeation cell was modified for the continuous flowing feed by connecting to a needle valve to control the upstream pressure. Besides, it is also equipped with a retentate channel to avoid the accumulation of feed at the upstream. Then the receiving volume of

permeation cell was connected to a gas chromatograph (GC) by a valve. Before permeation testing, GC was calibrated by one set of Messer gas mixtures of H_2 and N_2 with known composition to obtain the GC peak area as a function of gas mole fraction. The gas permeabilities of CO_2 and CH_4 are expressed by the following equations:

$$P_{H_2} = \frac{273 \times 10^{10}}{760} \frac{y_{H_2} Vl}{AT\left(\left(\frac{76}{14.7}\right) x_{H_2} P_2\right)} \frac{dp}{dt} \tag{5}$$

$$P_{N_2} = \frac{273 \times 10^{10}}{760} \frac{(1 - y_{H_2}) Vl}{AT\left(\left(\frac{76}{14.7}\right) (1 - x_{H_2}) P_2\right)} \frac{dp}{dt} \tag{6}$$

where P_{H_2} and P_{N_2} are the permeability (barrer) of H_2 and N_2, respectively. P_2 denotes the upstream feed gas pressure (atm), x refers to the mole fraction in the feed gas and y is the mole fraction in the permeate. The other symbols retain the same meanings as described earlier.

2.6. Measurements of gas sorption

Gas sorption behaviors of the 6FDA–durene and 6FDA–durene–GO membranes were measured *via* the dual-volume pressure decay method using XEMIS microbalance system. The membrane samples weighing about 50–60 mg was placed into the sample chamber and a vacuum was maintained for 3 h before sorption tests were conducted. Both the reference and sample chambers were immersed in the same water bath ((Techne FTE-10DE) from Techne Cambridge LTD (UK) with an accuracy of ±0.01 °C) to maintain the desired temperature. The sorption isotherm of each gas was obtained at 35 °C up to a maximum pressure of 10 atm. Since CO_2 would plasticize the membranes at high pressure, sorption tests were conducted in the order of H_2, O_2, N_2, CH_4 and then CO_2. The solubility coefficient was calculated from the slope of sorption isotherm since the sorption behavior obeyed the Henry's law. After that, the diffusion coefficient was calculated from solubility coefficient based on the equation of permeability (P) = diffusion coefficient (D) × solubility coefficient (S).

3. Results and discussion

3.1. Characterization of polymers

As presented in Fig. 1, a novel multi-permselective mixed matrix membrane was developed by incorporating versatile graphene oxide (GO) *via in situ* polymerization, which can improve the dispersion of GO into polyimide matrix. Here, the Lerf-Klinowski model GO has hydroxyl groups (–OH) and epoxy groups (–O–) on its surface, and carboxylic acid groups (–COOH) on the periphery of the basal graphitic platelets, as shown in Fig. 1. The Lerf-Klinowski model GO was a good candidate as a nanofiller in mixed matrix membranes because of its high aspect ratio, easy surface functionalization, and high thermal and mechanical properties. In order to improve the compatibility between GO and the polymer, the GO nanosheet was first interacted with durene, the carboxylic acid groups (–COOH) on

the edge of GO nanosheets reacted with amine groups of durene. After that the stoichiometric amount of 6FDA was added partially 3 times. The polyamic acid (PAA) consisting of GO solution was prepared under N_2 purge without moisture at room temperature. After reaction for 24 h, the viscous PAA–GO solution was cast on a Petri dish in the fume hood, as presented in Fig. 1. The thermal imidization process from PAA–GO to PI–GO was conducted in an oven under the heating stepwise at 100, 200 and 250 °C for 60, 60 and 30 min, respectively. The gas separation performance of PI–GO membranes was evaluated in the following session. The CMS membranes were prepared from PI-GO precursor at the carbonization temperatures from 500 °C to 600 °C. The structural change and fabrication process from PAA–GO-0.10% to PI–GO-0.10%, and thermally carbonized PI–GO-0.10%-550 °C were fully presented in Fig. 1.

The series of polyimide–graphene oxide membranes (PI–GO) were prepared *via in situ* polymerization. The TEM image in Fig. 1 shows the microstructure and high aspect ratio nanosheet. As shown in Fig. 2, GO was well dispersed in the polymer *via in situ* polymerization, with the increase of GO content, the viscous PAA–GO showed a significant change in color, and the color of PI–GO film is consistent with that of viscous PAA–GO solution. The chemical structures of PI were confirmed by FTIR spectra, as shown in Fig. 3(a), the characteristic imide absorption bands were observed at 1775 (asymmetric C=O stretching), 1720 (symmetric C=O stretching), 1390 (C–N stretching) and 735 cm^{-1} (C=O imide ring deformation).

The incorporation of GO will effectively restructure the architecture and have an immediate effect on polymer chain packing. Therefore, XRD was employed to investigate the evolution of the pore size as a function of the thermal treatment temperature. As revealed in Fig. 3(b), the original PI and PI–GO membranes had a peak at approximately 6.55 Å (micropore), which was probably attributed to the loosely packed polymer chains derived from the kinked backbone of polyimide. Here, the micro-pores were formed among the polymer chains. The next peak at 3.91 Å (ultra-micropore) was assigned to the *d*-spacing of the efficiently packed polymer chain-to-chain distance that contributes directly to the conformation of ultra-micropores. After thermal treatment at 500 °C, a new peak around 2.97 Å (ultrafine-micropore) gradually appeared, especially when the GO content increased from 0.5% to 1.0%. This means the polymer chain tends to have a much denser packing, at the same time, the partial carbonization or methyl (–CH$_3$) group degradation might occur in the membrane. In this process, the GO sheets help to create small ultrafine micropores. Clearly, the density of the other two peaks at 6.55 and 3.91 Å increase with increasing the GO content. The ultrafine-micropores (2.97 Å) play an important role for gas selectivity, while the micropores (6.55 Å) and ultra-micropores (3.91 Å) dominate the gas permeability. Here, the GO nanosheet could regulate the polymer arrangement *via* chemical bonds, and create many more micro-pores for gas transport. These XRD observations suggest that, the crystallites in carbon membranes
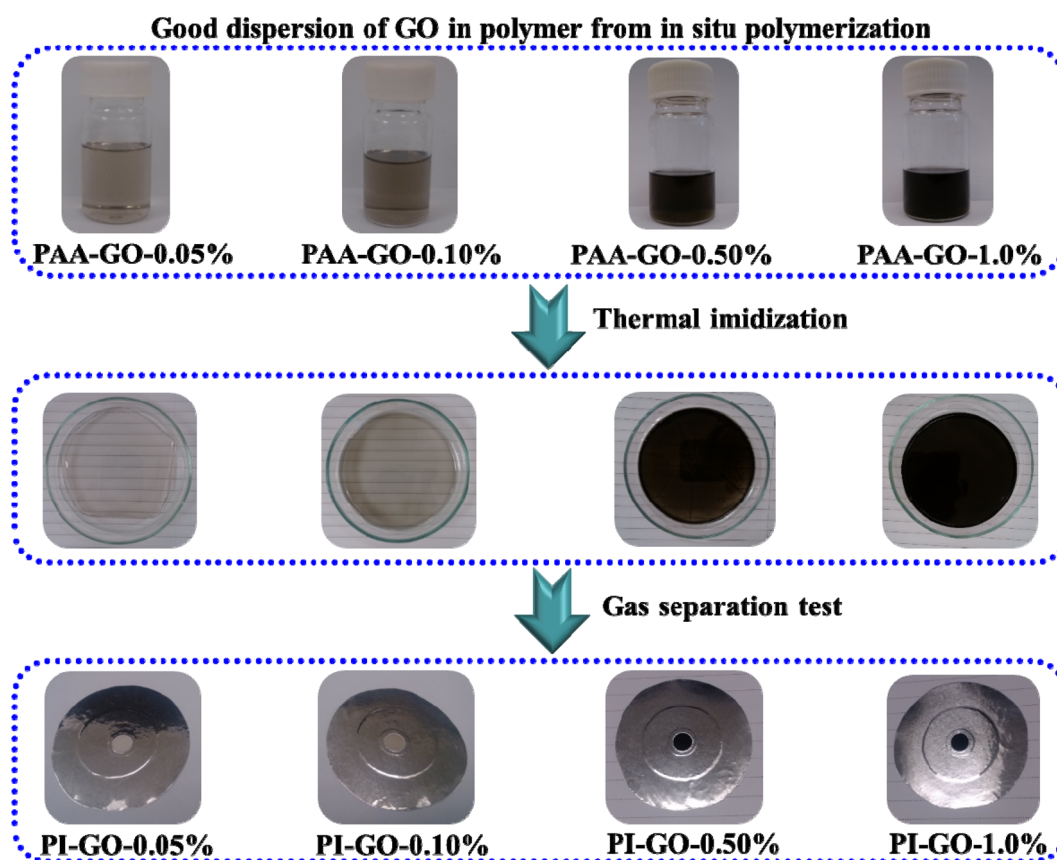

Fig. 2 The preparation of polyimide–graphene oxide membranes *via in situ* polymerization.
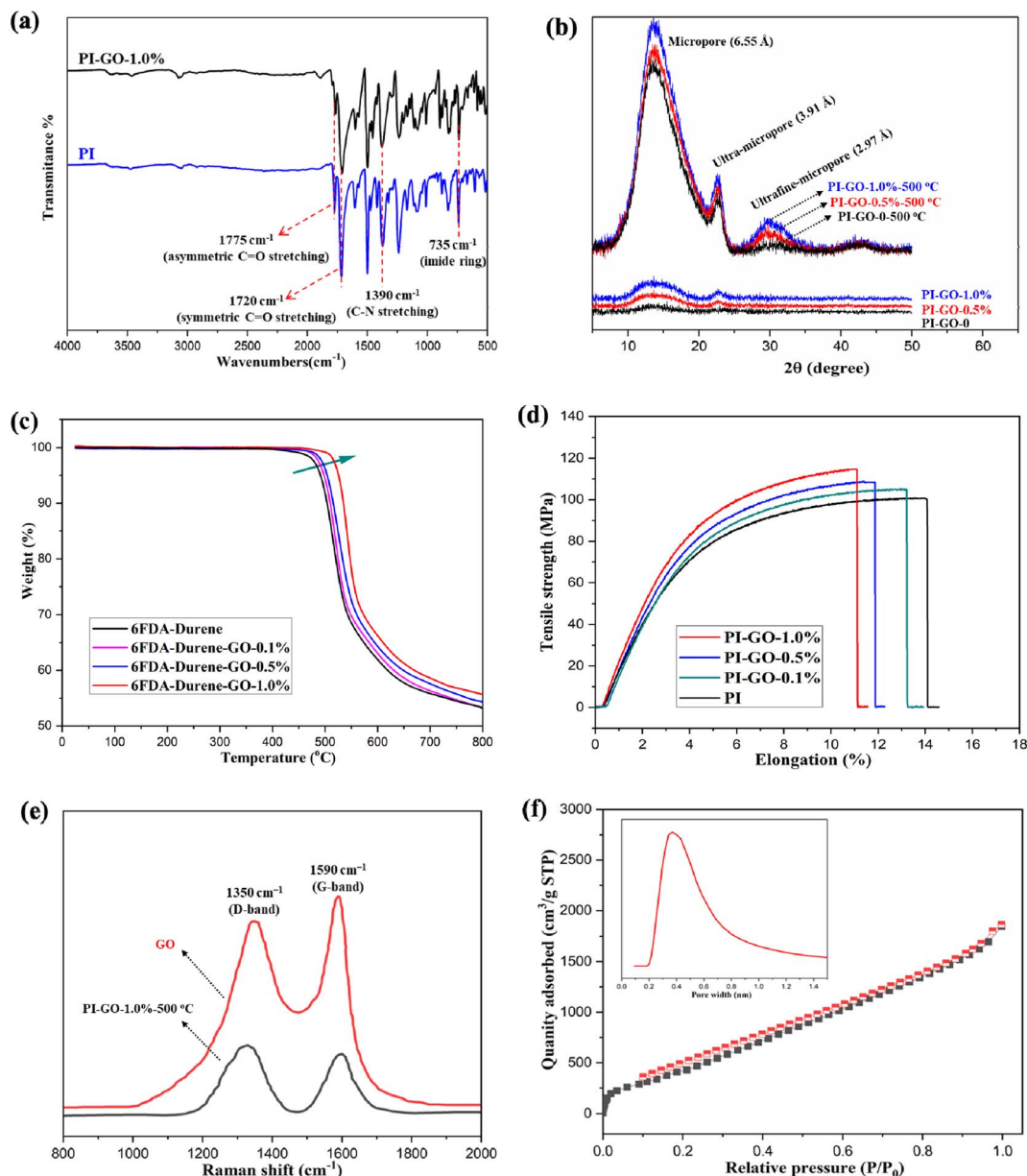
© 2023 The Author(s). Published by the Royal Society of Chemistry

Fig. 3 (a) FTIR spectra of PI and PI–GO membranes. (b) XRD spectra of PI and PI–GO membranes before and after thermal treatment. (c) TGA curves of the 6FDA–durene and 6FDA–durene–GO membranes in nitrogen at a heating rate of 10 °C min^{-1}. (d) Tensile strength of PI and PI–GO membranes. (e) Raman spectra of GO and PI–GO membranes. (f) BET specific surface area of the PI–GO-500 °C membrane.

have intermediate structures between graphite and amorphous states, also known as turbostratic structures or random layer lattice graphite structures.

As presented in Fig. 3(c), the thermal decomposition behaviors of pristine 6FDA–durene and 6FDA–durene–GO membranes as a function of temperature in a nitrogen atmosphere are shown in Fig. 3(c). To remove the moisture trapped in the membranes, all samples were dried at 100 °C for 8 h in a vacuum oven before the TGA test. From the TGA curves, it can be clearly seen that both 6FDA–durene and 6FDA–durene–GO membranes could withstand high temperatures, and there were no apparent weight loss until approximately 450 °C. The 6FDA–durene–GO membranes exhibit a slightly higher degradation

temperature than the 6FDA–durene membranes. The char yield also increased with increasing the GO loading content from 0.1% to 1% percent. The improved thermal stability was attributed to the incorporation of GO, which built strong carbon bridges between polyimide chains and strengthen the structural stability of the polymer matrix. The mechanical properties were evaluated by an Instron model 5542 at the speed of 10 mm min^{-1} with at least five film specimens (30 mm long, 5 mm wide, and about 0.05 mm thick), the results were averaged scan. As shown in Fig. 3(d), the stress–strain curves show that that PI–GO membranes were stronger than PI membranes. The mechanical properties of PI and PI–GO membranes are summarized in Table 1. The PI–GO composite films about 50

Table 1 The mechanical and thermal properties of graphene/polyimide nanocomposite films

Samples	Char yield[a] (%)	Tensile strength (MPa)	Young's moduli (MPa)	Elongation (%)	$T_{5\%}$[b] (°C)
PI	53.16	101	2231	14.1	491
PI–GO-0.1%	53.41	105	2565	13.2	498
PI–GO-0.5%	54.32	108	2911	11.9	504
PI–GO-1.0%	55.64	115	3354	11.2	525

[a] Residual weight (%) at 800 °C in nitrogen. [b] $T_{5\%}$ = 5% weight loss temperature (obtained by TGA at a heating rate of 10 °C min^{-1} in nitrogen).

μm thick are flexible and exhibit good mechanical properties. The tensile strengths and Young's modulus of PI–GO membranes are a little higher than the original PI, which is strengthen by GO bridge. As shown in Fig. 3(e), the Raman spectrum of GO exhibited bands at 1350 cm^{-1} and 1590 cm^{-1} due to the D and G bands, respectively. The functional groups on GO surface made some defects which led to D-band (disorders of sp^2 network) appearance while G-band represented sp^2-bonded carbon vibration. For PI–GO-1.0%-500 °C carbon membranes, the ratio of peak intensities (I_D/I_G) is 1.8, which is the typical degree of crystallinity (ordered carbon) for CMS membrane derived from precursor polymers. As shown in Fig. 3(f), the BET specific surface area of the PI-GO-500 °C membrane was 58 m^2 g^{-1}. The pore size distributions that were calculated from the corresponding adsorption isotherms by the NLDFT method, the PI–GO-500 °C membrane exhibited a peak centered at 0.36 nm.

As shown in Fig. 4, the photograph, cross section and surface morphology of the PI–GO CMS membranes were summarized

and compared. The internal microstructures of PI–GO CMS membranes were revealed by the cross-section SEM micrographs, which changed from smooth to rough with increasing the GO nanosheet contents. There was no apparent aggregation of GO, indicating its good compatibility with the polymer matrix. The top surface SEM images also indicated that the *in situ* polymerization of GO improved the interface compatibility between the GO nanosheets and polymer matrix.

3.2. Pure gas permeability and selectivity

The pure gas permeability and ideal selectivity of 6FDA–durene and 6FDA–durene–GO membranes are summarized in Table 2. When the loading content of GO increased, the permeability of H$_2$ increased slightly from 756 to 958. The permeability of N$_2$ increases from 65 to 69, with an increase of only 6%. To clearly elucidate the GO incorporation effect into the polymer matrix, Fig. 5 plots the gas separation performance (*i.e.*, H$_2$, O$_2$, N$_2$, CO$_2$ and CH$_4$) against the 2008 Robeson upper bound line. As shown
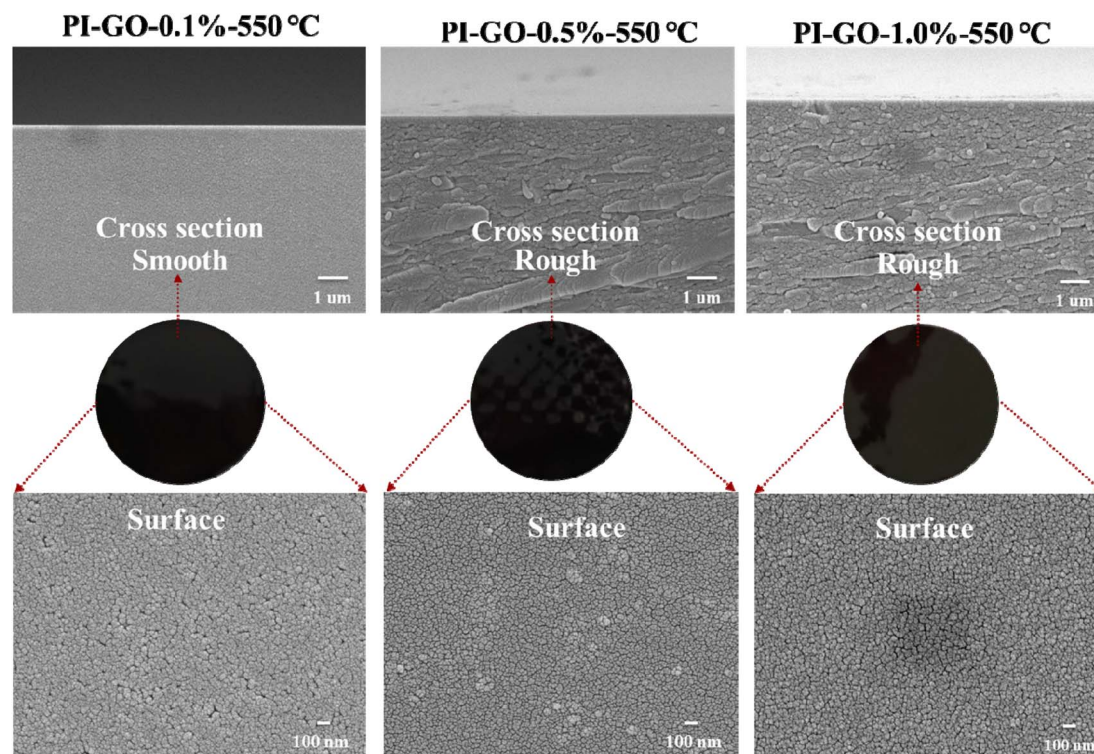

Fig. 4 Photograph, cross section and surface morphology of the PI–GO CMS membranes.

Paper

Table 2 Pure gas transport properties of the PI–GO and thermal treated PI–GO membranes

Membranes	Permeability (Barrer)					Selectivity		
	H_2	O_2	N_2	CO_2	CH_4	H_2/N_2	H_2/CO_2	H_2/CH_4
PI	756	211	65	959	58	11.59	0.79	12.90
PI–GO-0.1%	865	208	61	949	54	14.07	0.91	15.88
PI–GO-0.5%	919	227	67	1006	61	13.72	0.91	15.06
PI–GO-1.0%	958	231	69	1017	62	13.88	0.94	15.45
PI–GO-0.1%-500 °C	26 564	904	694	6954	478	38.29	3.82	55.52
PI–GO-0.5%-500 °C	23 412	745	539	5191	324	43.37	4.51	72.16
PI–GO-1.0%-500 °C	19 368	566	386	3446	243	50.16	5.62	79.80
PI–GO-0.1%-550 °C	11 107	972	113	1501	79	98.29	7.40	140.15
PI–GO-0.5%-550 °C	9625	749	90	1151	56	106.37	8.36	170.31
PI–GO-1.0%-550 °C	7462	508	64	748	35	116.82	9.97	210.42
PI–GO-0.1%-600 °C	2528	60	18	214	12	136.76	11.8	202.41
PI–GO-0.5%-600 °C	1993	44	13	134	8	154.56	14.9	236.76
PI–GO-1.0%-600 °C	1231	27	8	72	5	157.63	17.1	242.65

in Fig. 5, the permeability and selectivity of H_2 shift near to the upper bound lines with a small loading of graphene oxide. While the separation performance of 6FDA–durene–GO membranes for almost all of the pure gases could not surpass the 2008 Robeson upper bound line, even though, the permeability of all gases increased with increasing the GO loading content, while the selectivity of H_2/CO_2, H_2/N_2, and H_2/CH_4 just increased a little with the continuous loading of GO. It is because the high-aspect ratio GO nanosheets in polyimide matrix increase the length of the tortuous path of gas diffusion and generate a rigidified interface between the polymer matrix and fillers, which reduce the mobility of polymer chains and restrict the diffusion of larger molecules but favor the diffusion of small molecules H_2 with less resistance, thus improving gas diffusivity selectivity. In order to take full advantages of the GO nanosheets, the 6FDA–durene–GO membranes were treated at high temperature to improve the free volume and gas separation performance.

The pure gas permeabilities and ideal selectivities of PI–GO membranes carbonized at different temperatures for H_2, CO_2, O_2, N_2 and CH_4 were summarized in Table 2. The gas permeability followed the order of P (H_2) > P (CO_2) > P (O_2) > P (N_2) > P (CH_4), which was in reverse order of gas molecular size, indicating that the gas permeation of PI–GO CMS membranes was dominated by the molecular sieving mechanism. As the partial carbonization or methyl (–CH_3) group degradation occurred, the micropores (6.55 Å) and ultrafine micropores (2.97 and 3.91 Å) were generated after thermal treatment, which were confirmed from the XRD curves. Therefore, the gas permeability improved substantially after carbonization at high temperature. The H_2 permeability of PI–GO-0.1%-500 °C was almost 30 times higher than that of the original PI–GO-0.1% membrane. As the pyrolysis temperature increased, the gas permeabilities of all gases were gradually reduced. When the carbonization temperature was raised from 500 to 600 °C, however, the average reduction rate of gas permeability increased with increasing of gas molecular size, such as H_2 < CO_2 < O_2 < N_2 < CH_4, which resulted in a gradual increase in the ideal selectivities for H_2/N_2, H_2/CH_4, and H_2/CO_2 gas pairs. This result could

be attributed to the shrinkage of the pore structure that greatly restricted the diffusion of larger gas molecules. In particular, the PI–GO-1.0%-600 °C membrane exhibited extraordinarily high H_2/N_2 (157) and H_2/CH_4 (243) selectivity, which was related to its interlayer spacing of GO nanosheet being much smaller than the molecular size of N_2 and CH_4, as confirmed by the above XRD results.

After high-temperature treatment over 500 °C, the partial carbonization or methyl (–CH_3) group degradation occurred, which was confirmed from the TGA degradation curves. As a result, a lightly cross-linked and rigid polymer networks were generated under the guidance of 2D GO nanosheets. In the high-temperature treatment process, the GO nanosheets would regulate the packing of polymer chain, and manipulate the free volume of 6FDA–durene–GO membranes. This process would generate more micropores (6.55 Å) and ultrafine micropores (2.97 and 3.91 Å), which improved the gas permeability and selectivity. The dimensions of the ultrafine micropores (2.97 and 3.91 Å) could discern the gas kinetic diameters (2.89–3.8 Å). As a result, the gas selectivity was mainly determined by ultrafine micropores, while the gas permeability was largely related to the micropores (6.55 Å). As presented in Fig. 5, both the gas permeability and selectivity were improved substantially after thermal treatment, and the separation performance of 6FDA–durene–GO-500 °C for almost all gas pairs could surpass the 2008 Robeson upper bound line. After thermal treatment at 500 and 550 °C for 1 h, the selectivity of H_2/CO_2, H_2/N_2, and H_2/CH_4 increased by one order of magnitude. As the carbonization temperature increased, ultrahigh selectivities for H_2/CO_2 (17), H_2/N_2 (157), and H_2/CH_4 (243) gas pairs were achieved while maintaining moderate H_2 gas permeabilities. The excellent gas separation performance of the prepared CMS membranes may be attributed to the guidance of 2D GO nanosheets and the structural evolution during pyrolysis. The major transport pathway for gas molecules might be the structural pores within GO flakes, and the gas selectivity was probably due to the interlayer spacing between GO nanosheets. It's sure that the PI–GO based CMS membranes for H_2/N_2, H_2/CH_4, and H_2/CO_2 gas pairs can produce high purity hydrogen, and the high H_2
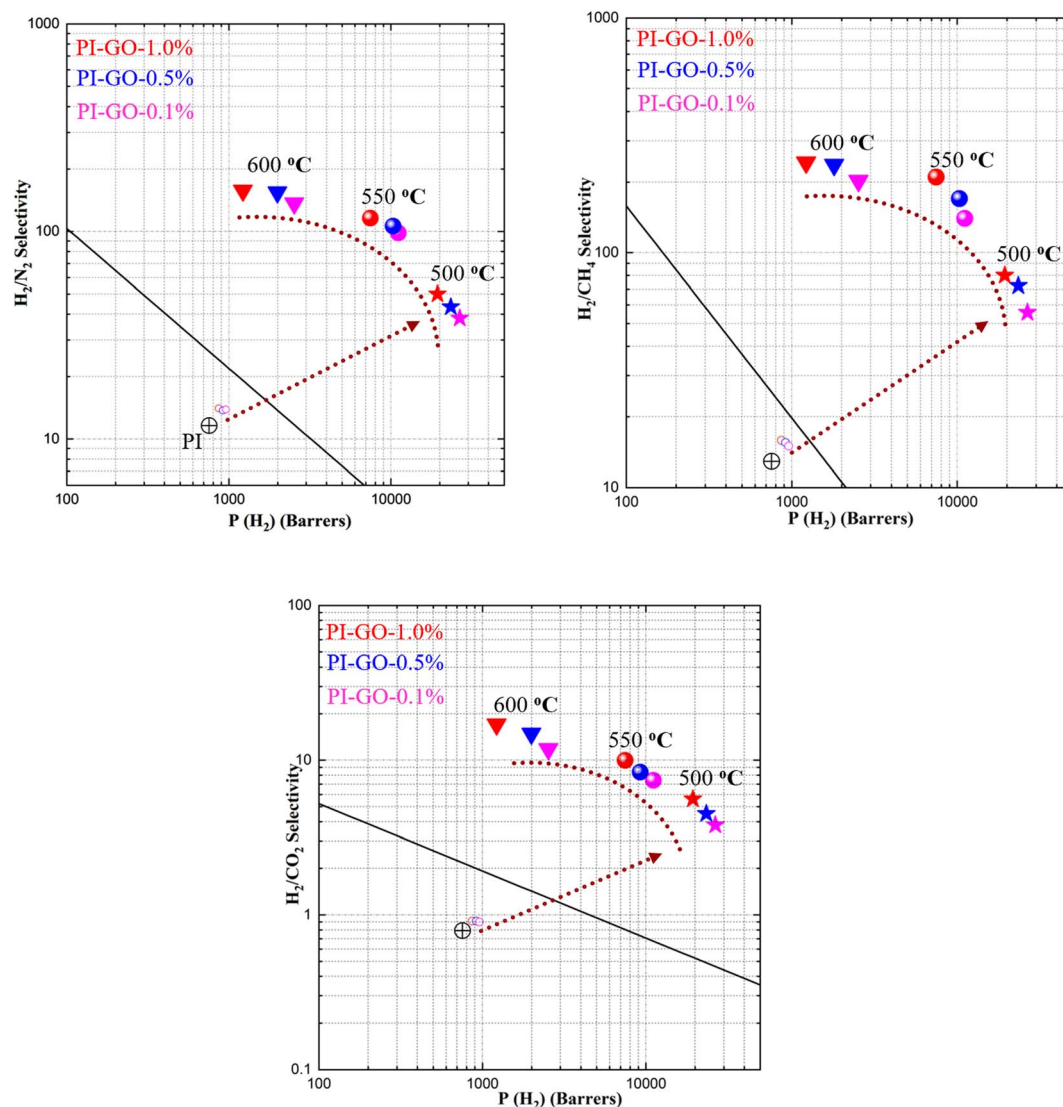
Fig. 5 Gas separation performance of the PI–GO and thermal treated PI–GO membranes at 35 °C and 3.5 atm.

permeability will achieve competitive separation costs. Therefore, the novel CMS membranes derived from PI–GO polymeric precursor offer great application potential in hydrogen purification.

3.3. Mixed gas permeability and selectivity

To further evaluate the feasibility of PI–GO CMS membranes, the gas separation performance for binary gas mixtures of H_2/N_2 (50%/50%) was also tested. As presented in Fig. 6, both pure gas and mixed gas separation performance could overcome the 2008 Robeson upper bound line. The H_2 permeability and corresponding selectivity in mixed-gas experiments were lower than those obtained in pure-gas experiments under the same conditions. This phenomenon can be ascribed to the competitive sorption effect of mixed gases on the fixed Langmuir sorption sites, and the affinity of CO_2, N_2 and CH_4 for the sorption sites overwhelms H_2. As demonstrated in Fig. 6, the H_2/CH_4 selectivity under mixed-gas conditions was slightly lower

than the ideal selectivity under pure-gas conditions at the feed pressure of 3.5 atm. This phenomenon was due to a combination of competitive sorption (reduction in H_2 permeability) and plasticization (increase in CH_4 permeability). Similar behavior was also observed in other reported membranes.[47] Surprisingly, the PI–GO-1.0%-600 °C membrane displayed ultrahigh H_2/N_2 (157) and H_2/CH_4 (243) selectivity, which were better than those of state-of-the-art PEI, PPO, PIM-700 °C, TB-800 °C, glucose, PIM–6FDA–OH-630 °C, PIM–6FDA–OH-800 °C, and some polyimide membranes.

The gas permeability and selectivity are two important parameters used to evaluate membrane separation performance. The gas permeability followed the order of $P(H_2) > P(CO_2) > P(O_2) > P(N_2) > P(CH_4)$, which was in reverse order of the gas kinetic diameter, indicating that the gas permeation of PI–GO CMS membranes was dominated by the molecular-sieving mechanism. The ultrahigh H_2/N_2 (117) gas selectivity was probably due to the interlayer spacing between GO
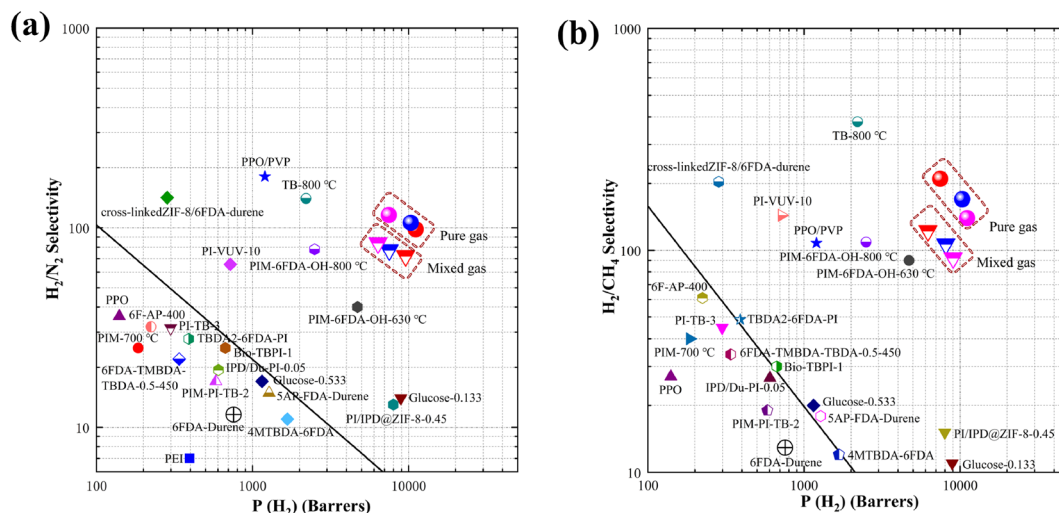
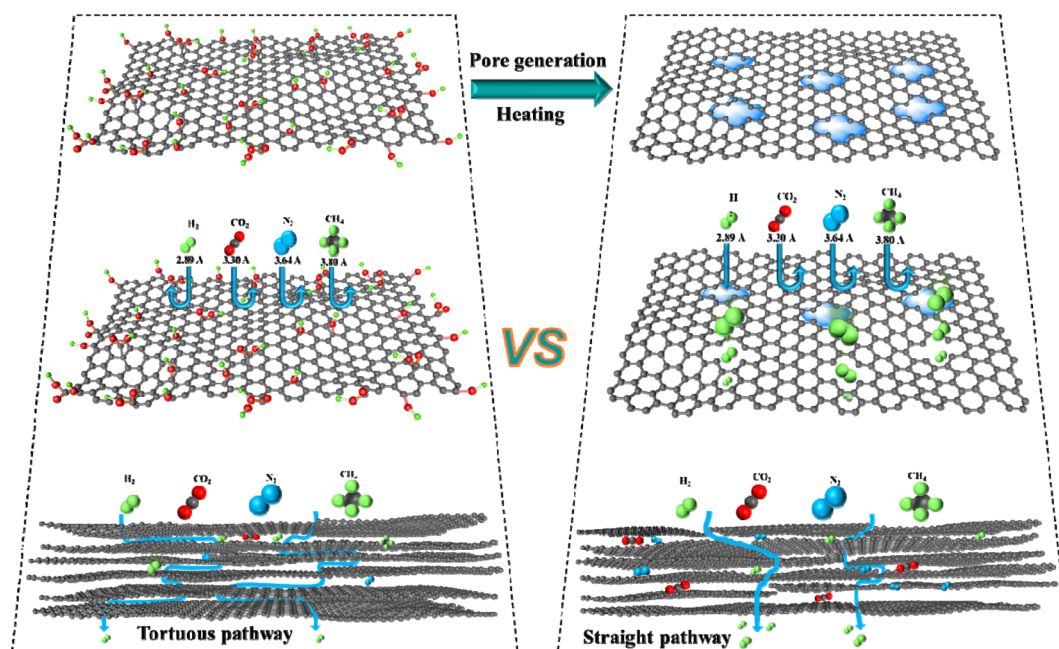**Fig. 6** Gas separation performance of the thermal treated PI–GO membranes.

Fig. 7 Mixed gas separation performance of the thermal treated PI–GO membranes.

nanosheets and selective structural pores within PI–GO membrane after thermal treatment. As presented in Fig. 7, there are more straight and upright pathways after thermal treatment, compared with the tortuous pathways through parallel-stacked GO nanosheets. Before thermal treatment, the H_2 permeability and H_2/N_2 selectivity of PI–GO-1.0% were only 958 Barrer and 13.88, respectively. While, after thermal treatment, the H_2 permeability of PI–GO-1.0%-500 °C membrane increased up to 19 368 Barrer, which was approximately 20 times higher than that of the pristine PI–GO-1.0% membrane. At the same time, the H_2/N_2 selectivity of PI–GO-1.0%-500 °C increased to 50.16, which was 3.6 times higher than that of the original membrane. The great increase of both permeability and

selectivity were due to the pore generation in GO nanosheets and polymer matrix after thermal treatment. Therefore, the major transport pathways for these gas molecules might be the free volume from the partial degradation of polyimide and selective structural pores within GO flakes after thermal treatment.

3.4. Gas sorption

The gas sorption behaviors of 6FDA–durene and 6FDA–durene–GO membranes were analyzed *via* the dual-volume pressure decay method using the XEMIS microbalance system. The gas sorption isotherms of the PI–GO and PI–GO-500 °C membranes are presented in Fig. 8. It's clear to see that the gas
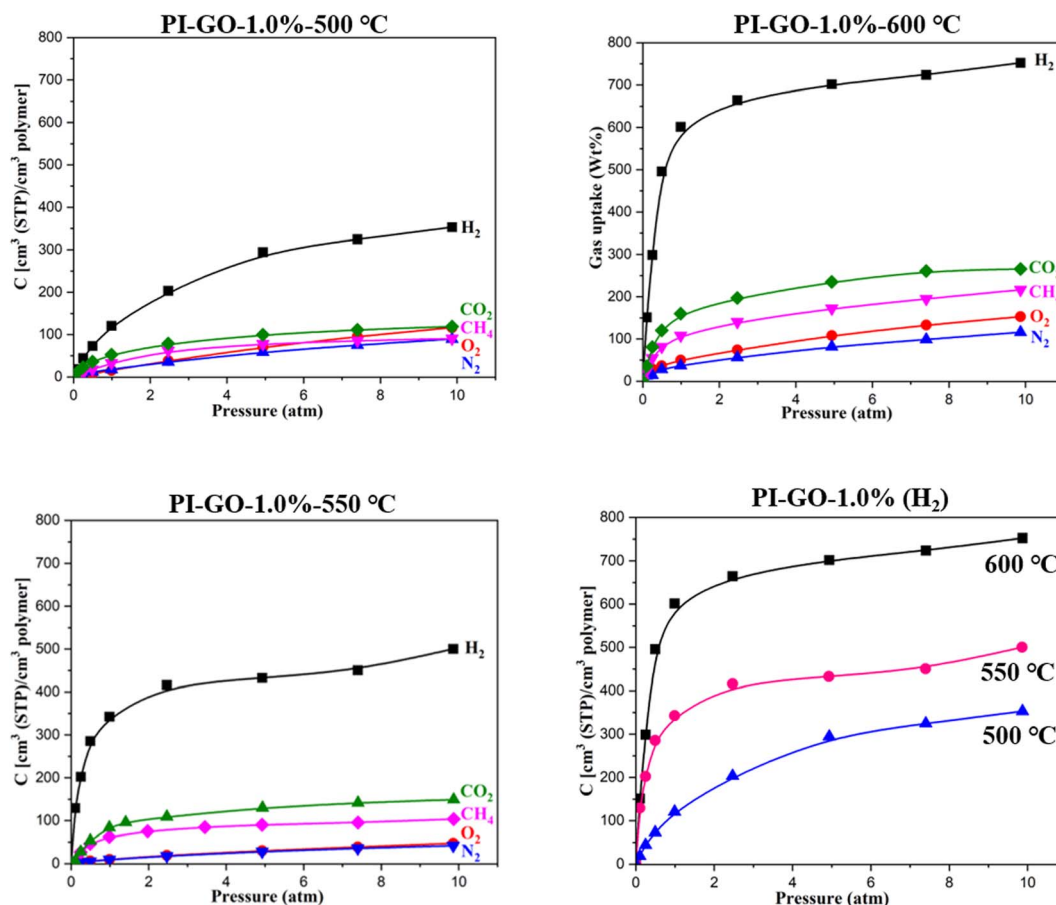
Fig. 8 Gas sorption isotherms of the thermal treated PI–GO membranes.

concentrations to the pressure axis are convex curves, the non-linear sorption behaviors agree well with the typical trend of polymeric membranes that can be described by the so-called dual sorption model. Henry's law mode believes that the gas absorbed in membrane is similar to gas molecules dissolved in a rubbery polymer where the sorption concentration linearly increases with increasing the pressure. While the Langmuir mode considers that the gas sorption in membrane has a capacity limit because it behaves like a hole-filling process.[48,49] Therefore, the gas sorption behaviors of PI and PI–GO membranes follow the dual sorption mode (Henry's law mode and Langmuir mode). So as can be clearly seen from Fig. 8, the gas concentrations increase nonlinearly with increasing the gas feeding pressure up to 10 bar. For the same gas, the gas concentration in different membranes follows the order of PI–GO-1.0% > PI–GO-0.5% > PI–GO-0.1% > PI, since membranes with higher content of GO, which can effectively restructure the architecture, have more micropores to capture gas molecules. After thermal treatment, the gas concentration increases considerably and follows the order of PI–GO-1.0%-500 °C > PI–GO-0.5%-500 °C > PI–GO-0.1%-500 °C > PI, the degradation of sensitive groups on GO nanosheets could create more micropores to hold gas molecules. The gas concentration increases with increasing temperature and follows the order of PI–GO-1.0%-600 °C > PI–GO-0.5%-550 °C > PI–GO-0.1%-500 °C, more

micropores would be created at higher temperature. While for the same membrane, the H_2 has the highest sorption capability, the concentrations of different gases follow the order of $H_2 > CO_2 > CH_4 > O_2 > N_2$, that's probably because the graphite structure from the decomposition of polymer and GO have a strong affinity with H_2 gas molecules.

The solubility coefficient could be calculated from this equation $S = c/p$, and is in the form of a secant slope from the sorption isotherm at a certain pressure. As observed in Fig. 8, the solubility coefficients increase with increasing the GO content. As the temperature increases, the solubility coefficients increase especially for H_2 gas, which is approximately 5 times higher than the N_2, CO_2, and CH_4. The corresponding solubility coefficients and diffusion coefficients at 3.5 atm are listed in Table 3. Compared with the pristine PI membrane, the incorporation of GO into PI polymer matrix improves the solubility coefficients, and after thermal treatment, the PI–GO membranes have improved solubility coefficients and diffusion coefficients simultaneously. Thus, the gas permeability of pristine PI–GO membrane increases with increasing the GO content, and the gas selectivity of the thermally treated PI–GO membrane increases with increasing the temperature from 500 °C to 600 °C. As the carbonization temperature increased, the gas sorption capability of CMS membranes increased rapidly and followed the order of PI–GO-1.0%-600 °C > PI–GO-

Table 3 Permeability, solubility and diffusion coefficients of the thermal treated PI–GO-1.0% membranes

Membranes	Solubility coefficient (cm³ (STP)/cm³ polymer atm)					Diffusivity coefficient (×10⁷ cm² s⁻¹)				
	H_2	CO_2	CH_4	O_2	N_2	H_2	CO_2	CH_4	O_2	N_2
PI–GO-1.0%-500 °C	65	26	19	15	12	23	22	0.9	2.9	2.4
PI–GO-1.0%-550 °C	120	34	23	18	16	4.6	3.7	0.2	2.1	0.3
PI–GO-1.0%-600 °C	194	61	44	25	19	0.5	0.2	0.1	0.1	0.1

1.0%-550 °C > PI–GO-1.0%-500 °C. The H_2 molecules had better interactions with the ordered graphite structure than with the turbostratic polymeric structure.

4. Conclusions

Graphene oxide tuned polyimide hydrogen purification membranes were prepared from *in situ* polymerization. The ultraselective CMS membranes for H_2/N_2, H_2/CH_4 and H_2/CO_2 binary gas were prepared from the PI–GO precursor at carbonization temperatures of 500–600 °C. Compared with the original PI–GO membranes, both the H_2/N_2, H_2/CH_4, H_2/CO_2 selectivity and H_2 permeability greatly increased after thermal treatment at high temperature. The gas permeability followed the order of $P(H_2) > P(CO_2) > P(O_2) > P(N_2) > P(CH_4)$, which was in reverse order of gas molecular size, indicating that the gas permeation of PI–GO CMS membranes was dominated by the molecular sieving mechanism. In the thermal carbonization process, the turbostratic polymeric structure gradually became denser and more ordered carbon structure under the guidance of 2D GO nanosheets. More ultrafine-micropores (2.97 Å) were created for improved H_2 selectivity, while the micropores (6.55 Å) and ultra-micropores (3.91 Å) dominated the gas permeability. As the carbonization temperature increased, the gas sorption capability of CMS membranes increased and followed the order of PI–GO-1.0%-600 °C > PI–GO-1.0%-550 °C > PI–GO-1.0%-500 °C, and the H_2 molecules had better interaction with the ordered graphite structure than the turbostratic polymeric structure. Therefore, the H_2/N_2, H_2/CH_4, and H_2/CO_2 selectivity increased owing to the substantial enhancement of diffusion and solubility selectivity. The PI–GO-1.0%-550 °C membrane exhibited an ultrahigh H_2/N_2 selectivity of 117 and H_2 permeability of 7462 Barrer. The CMS membranes with ultrahigh gas selectivity and permeability have bright application prospects in hydrogen purification.

Conflicts of interest

There are no conflicts to declare.

Acknowledgements

References

1 G. W. Crabtree and M. S. Dresselhaus, The hydrogen fuel alternative, *MRS Bull.*, 2011, **33**, 421–428.

2 N. W. Ockwig and T. M. Nenoff, Membranes for hydrogen separation, *Chem. Rev.*, 2007, **107**(10), 4078–4110.

3 H. Li, Z. Song, X. Zhang, Y. Huang, S. Li, Y. Mao, H. J. Ploehn, Y. Bao and M. Yu, Ultrathin, molecular-sieving graphene oxide membranes for selective hydrogen separation, *Science*, 2013, **342**(6154), 95–98.

4 F. G. Kerry, *Industrial gas handbook: gas separation and purification*, Taylor and Franc Group, New York, 2006.

5 W. Liu, S. D. Jiang, Y. Yan, W. Wang, J. Li, K. Leng and K. P. Loh, A solution-processable and ultra-permeable conjugated microporous thermoset for selective hydrogen separation, *Nat. Commun.*, 2020, **11**(1), 1–8.

6 H. B. Park, J. Kamcev, L. M. Robeson, M. Elimelech and B. D. Freeman, Maximizing the right stuff: the trade-off between membrane permeability and selectivity, *Science*, 2017, **356**(6343), eaab0530.

7 M. X. Shan, X. L. Liu, X. R. Wang, I. Yarulina, B. Seoane, F. Kapteijn and J. Gascon, Facile manufacture of porous organic framework membranes for precombustion CO_2 capture, *Sci. Adv.*, 2018, **4**(9), eaau1698.

8 L. X. Zhu, M. T. Swihart and H. Q. Lin, Unprecedented size-sieving ability in polybenzimidazole doped with polyprotic acids for membrane H_2/CO_2 separation, *Energy Environ. Sci.*, 2018, **11**(1), 94–100.

9 H. W. Kim, H. W. Yoon, S. M. Yoon, B. M. Yoo, B. K. Ahn, Y. H. Cho, H. J. Shin, H. C. Yang, U. Paik, S. Kwon, J. Y. Choi and H. B. Park, Selective gas transport through few-layered graphene and graphene oxide membranes, *Science*, 2013, **342**(6154), 91–95.

10 A. Achari, S. Sahaha and M. Eswaramoorthy, High performance MoS_2 membranes: effects of thermally driven phase transition on CO_2 separation efficiency, *Energy Environ. Sci.*, 2016, **9**(4), 1224–1228.

11 Y. Peng, Y. S. Li, Y. J. Ban, W. M. Jiao, X. L. Liu and W. S. Yang, Metal-organic framework nanosheets as building blocks for molecular sieving membranes, *Science*, 2014, **346**(6215), 1356–1359.

12 Z. X. Kang, M. Xue, L. L. Fan, L. Huang, L. J. Guo, G. Y. Wei, B. L. Chen and S. L. Qiu, Highly selective sieving of small gas molecules by using an ultra-microporous metal-organic framework membrane, *Energy Environ. Sci.*, 2014, 7(12), 4053–4060.

13 F. Cacho-Bailo, I. Matito-Martos, J. Perez-Carbajo, M. Etxeberría-Benavides, O. Karvan, V. Sebastián, S. Calero, C. Téllez and J. Coronas, On the molecular mechanisms for the H_2/CO_2 separation performance of zeolite imidazolate framework two-layered membranes, *Chem. Sci.*, 2017, **8**(1), 325–333.

14 A. S. Huang, W. Dou and J. Caro, Steam-stable zeolitic imidazolate framework ZIF-90 membrane with hydrogen selectivity through covalent functionalization, *J. Am. Chem. Soc.*, 2010, **132**(44), 15562–15564.

15 H. W. Fan, M. H. Peng, I. Strauss, A. Mundstock, H. Meng and J. Caro, High-flux vertically aligned 2D covalent organic framework membrane with enhanced hydrogen separation, *J. Am. Chem. Soc.*, 2020, **142**(15), 6872–6877.

16 L. Q. Hu, V. T. Bui, A. Krishnamurthy, S. H. Fan, W. J. Guo, S. Pal, X. Y. Chen, G. Y. Zhang, Y. F. Ding, R. P. Singh, M. Lupion and H. Q. Lin, Tailoring sub-3.3 Å ultramicropores in advanced carbon molecular sieve membranes for blue hydrogen production, *Sci. Adv.*, 2022, **8**(10), eabl8160.

17 L. M. Robeson, The upper bound revisited, *J. Membr. Sci.*, 2008, **320**(1–2), 390–400.

18 B. D. Freeman, Basis of permeability/selectivity tradeoff relations in polymeric gas separation membranes, *Macromolecules*, 1999, **32**(2), 375–380.

19 J. Kurchan, In and out of equilibrium, *Nature*, 2005, **433**(7023), 222–225.

20 Q. L. Song, S. Cao, R. H. Pritchard, B. Ghalei, S. A. Al-Muhtaseb, E. M. Terentjev, A. K. Cheetham and E. Sivaniah, Controlled thermal oxidative crosslinking of polymers of intrinsic microporosity towards tunable molecular sieve membranes, *Nat. Commun.*, 2014, **5**(1), 1–12.

21 S. M. Saufi and A. F. Ismail, Fabrication of carbon membranes for gas separation-a review, *Carbon*, 2004, **42**(2), 241–259.

22 L. F. Lei, F. J. Pan, A. Lindbråthen, X. P. Zhang, M. Hillestad, Y. Nie, L. Bai, X. Z. He and M. D. Guiver, Carbon hollow fiber membranes for a molecular sieve with precise-cutoff ultramicropores for superior hydrogen separation, *Nat. Commun.*, 2021, **12**(1), 1–9.

23 O. Sanyal, C. Zhang, G. B. Wenz, S. L. Fu, N. Bhuwania, L. R. Xu, M. Rungta and W. J. Koros, Next generation membranes-using tailored carbon, *Carbon*, 2018, **127**, 688–698.

24 L. F. Lei, L. Bai, A. Lindbråthen, F. J. Pan, X. P. Zhang and X. Z. He, Carbon membranes for CO_2 removal: Status and perspectives from materials to processes, *Chem. Eng. J.*, 2020, **401**, 126084.

25 L. Liu, D. X. Liu and C. Zhang, High-temperature hydrogen/propane separations in asymmetric carbon molecular sieve hollow fiber membranes, *J. Membr. Sci.*, 2022, **642**, 119978.

26 X. Z. He, L. F. Lei and Z. D. Dai, Green hydrogen enrichment with carbon membrane processes: Techno-economic feasibility and sensitivity analysis, *Sep. Purif. Technol.*, 2021, **276**, 119346.

27 X. Z. He, Techno-economic feasibility analysis on carbon membranes for hydrogen purification, *Sep. Purif. Technol.*, 2017, **186**, 117–124.

28 M. J. Hou, L. Li, Z. L. He, R. S. Xu, Y. H. Lu, J. H. Zhang, Z. L. Pan, C. W. Song and T. H. Wang, High-performance carbon molecular sieving membrane derived from a novel hydroxyl-containing polyetherimide precursor for CO_2 separations, *J. Membr. Sci.*, 2022, **656**, 120639.

29 M. J. Hou, W. B. Qi, L. Li, R. S. Xu, J. J. Xue, Y. Y. Zhang, C. W. Song and T. H. Wang, Carbon molecular sieve membrane with tunable microstructure for CO_2 separation: Effect of multiscale structures of polyimide precursors, *J. Membr. Sci.*, 2021, **635**, 119541.

30 W. L. Qiu, J. Vaughn, G. P. Liu, L. R. Xu, M. Brayden, M. Martinez, T. Fitzgibbons, G. Wenz and W. J. Koros, Hyperaging tuning of a carbon molecular-sieve hollow fiber membrane with extraordinary gas-separation performance and stability, *Angew. Chem., Int. Ed.*, 2019, **58**(34), 11700–11703.

31 K. H. Li, Z. Y. Zhu, H. Dong, Q. X. Li, W. H. Ji, J. X. Li, B. W. Cheng and X. H. Ma, Bottom up approach to study the gas separation properties of PIM-PIs and its derived CMSMs by isomer monomers, *J. Membr. Sci.*, 2021, **635**, 119519.

32 P. H. Tchoua Ngamou, M. E. Ivanova, O. Guillon and W. A. Meulenberg, High-performance carbon molecular sieve membranes for hydrogen purification and pervaporation dehydration of organic solvents, *J. Mater. Chem. A*, 2019, **7**(12), 7082–7091.

33 C. Zhang and W. J. Koros, Ultraselective carbon molecular sieve membranes with tailored synergistic sorption selective properties, *Adv. Mater.*, 2017, **29**(33), 1701631.

34 X. H. Ma, R. Swaidan, B. Y. Teng, H. Tan, O. Salinas, E. Litwiller, Y. Han and I. Pinnau, Carbon molecular sieve gas separation membranes based on an intrinsically microporous polyimide precursor, *Carbon*, 2013, **62**, 88–96.

35 X. W. Chen, J. J. Eugene Chong, Z. W. Celine Fah and L. Hong, Glucose-derived carbon molecular sieve membrane: An inspiration from cooking, *Carbon*, 2017, **111**, 334–337.

36 R. S. Xu, L. He, L. Li, M. J. Hou, Y. Z. Wang, B. S. Zhang, C. H. Liang and T. H. Wang, Ultraselective carbon molecular sieve membrane for hydrogen purification, *J. Energy Chem.*, 2020, **50**, 16–24.

37 T. H. Wang, B. Zhang, J. S. Qiu, Y. H. Wu, S. H. Zhang and Y. M. Cao, Effects of sulfone/ketone in poly (phthalazinone ether sulfone ketone) on the gas permeation of their derived carbon membranes, *J. Membr. Sci.*, 2009, **330**(1–2), 319–325.

38 S. L. Liu, T. H. Wang, Q. L. Liu, S. H. Zhang, Z. C. Zhao and C. H. Liang, Gas permeation properties of carbon molecular sieve membranes derived from novel poly (phthalazinone ether sulfone ketone), *Ind. Eng. Chem. Res.*, 2008, **47**(3), 876–880.

39 T. H. Weng, H. H. Tseng, G. L. Zhuang and M. Y. Wey, Development of CMS/Al_2O_3-supported PPO composite

membrane for hydrogen separation, *Int. J. Hydrogen Energy*, 2013, **38**(7), 3092–3104.

40 A. K. Itta, H. H. Tseng and M. Y. Wey, Fabrication and characterization of PPO/PVP blend carbon molecular sieve membranes for H_2/N_2 and H_2/CH_4 separation, *J. Membr. Sci.*, 2011, **372**(1–2), 387–395.

41 M. Omidvar, H. Nguyen, H. Liang, C. M. Doherty, A. J. Hill, C. M. Stafford, X. S. Feng, M. T. Swihart and H. Q. Lin, Unexpectedly strong size-sieving ability in carbonized polybenzimidazole for membrane H_2/CO_2 separation, *ACS Appl. Mater. Interfaces*, 2019, **11**(50), 47365–47372.

42 A. K. Itta and H. H. Tseng, Hydrogen separation performance of CMS membranes derived from the imide-functional group of two similar types of precursors, *Int. J. Hydrogen Energy*, 2011, **36**(14), 8645–8657.

43 M. Kiyono, P. J. Williams and W. J. Koros, Effect of polymer precursors on carbon molecular sieve structure and separation performance properties, *Carbon*, 2010, **48**(15), 4432–4441.

44 H. B. Park, Y. K. Kim, J. M. Lee, S. Y. Lee and Y. M. Lee, Relationship between chemical structure of aromatic polyimides and gas permeation properties of their carbon molecular sieve membranes, *J. Membr. Sci.*, 2004, **229**(1–2), 117–127.

45 K. Hazazi, X. H. Ma, Y. G. Wang, W. Ogieglo, A. Alhazmi, Y. Han and I. Pinnau, Ultra-selective carbon molecular sieve membranes for natural gas separations based on a carbon-rich intrinsically microporous polyimide precursor, *J. Membr. Sci.*, 2019, **585**, 1–9.

46 M. J. Hou, L. Li, J. Song, R. S. Xu, Z. L. He, Y. H. Lu, Z. L. Pan, C. W. Song and T. H. Wang, Polyimide-derived carbon molecular sieve membranes for high-efficient hydrogen purification: The development of a novel phthalide-containing polyimide precursor, *Sep. Purif. Technol.*, 2022, **301**, 121982.

47 J. T. Liu, Y. C. Xiao, K. S. Liao and T. S. Chung, Highly permeable and aging resistant 3D architecture from polymers of intrinsic microporosity incorporated with beta-cyclodextrin, *J. Membr. Sci.*, 2017, **523**, 92–102.

48 P. Li, T. S. Chung and D. R. Paul, Gas sorption and permeation in PIM-1, *J. Membr. Sci.*, 2013, **432**, 50–57.

49 P. Li, D. R. Paul and T. S. Chung, High performance membranes based on ionic liquid polymers for CO_2 separation from the flue gas, *Green Chem.*, 2012, **14**(4), 1052–1063.